Inorg. Chem. **2008**, *47*, 8935−8942

Inorganic Chemistry
Article

Novel 3-D PtS-like Tetrazolate-Bridged Manganese(II) Complex Exhibiting Spin-Canted Antiferromagnetism and Field-Induced Spin-Flop Transition

Ying-Bing Lu,[†,‡] Ming-Sheng Wang,[†] Wei-Wei Zhou,[†] Gang Xu,[†] Guo-Cong Guo,*[,†] and Jin-Shun Huang[†]

State Key Laboratory of Structural Chemistry, Fujian Institute of Research on the Structure of Matter, Chinese Academy of Sciences, Fuzhou, Fujian 350002, People's Republic of China, and Graduate School of the Chinese Academy of Sciences, Beijing 100039, People's Republic of China

Received June 4, 2008

Two novel manganese(II) tetrazolate coordination polymers, $Mn_3(Hbta)_4(\mu_2\text{-}OH)_2(H_2O)\cdot 2H_2O$ (**1**) and $Mn(bta)(H_2O)$ (**2**), were obtained by the hydrothermal reaction of $MnCl_2\cdot 4H_2O$ with *N*,*N*-bis[1(2)*H*-tetrazol-5-yl]amine (H_2bta) in different pH values. Compound **1** exhibits a 2-D (4,4) layer structure, which is built from binuclear $Mn_2(\mu_2\text{-}OH)_2$ subunits and μ_3-bridging $Hbta^-$ linkers. Compound **2** is a helical framework, and its 3-D PtS-like net is constructed by $Mn_2(bta)_2$ dimers and μ_5-bridging bta^{2-} linkers. Magnetic measurements reveal that compound **1** displays an antiferromagnetic ordering, while compound **2** exhibits the coexistence of a spin-canted antiferromagnetic coupling and a field-induced spin-flop transition.

Introduction

Considerable current interest is focused on the preparation and study of molecular-based magnetic materials because of their great value in investigating complex magnetostructural relationships and some fundamentally magnetic behaviors.[1] In particular, molecular magnetism with spontaneous magnetization, such as spin canting and metamagnetism, is continously pursued for its potential application as molecular magnets.[2] However, the design and preparation of such molecular magnetic materials are still a challenging topic. The common synthetic approach of molecular magnetic materials is to incorporate paramagnetic centers with suitable bridging ligands to fabricate polynuclear complexes or extended networks that can give rise to magnetic exchange coupling. Besides the nature of the metal centers, the nature and the linking modes of the bridging ligand also play a crucial role in the whole magnetic system; therefore, the search and exploration of an appropriate ligand is a long-standing task.[3]

As bridging ligands, five-membered heterocyclic azoles (pyrazoles, imidazoles, triazoles, tetrazoles, etc.) and their derivatives have drawn much attention because of their strong σ-electron donors to metals and their diverse coordination modes, forming numerous multidimensional coordination complexes with intriguing topologies.[4] They have also shown to be potential candidates to construct molecular magnets, exhibiting various bulk magnetic behaviors such as antiferromagnetism, ferromagnetism, spin crossover, spin canting,

* To whom correspondence should be addressed. E-mail: gcguo@fjirsm.ac.cn. Fax: 86 591 83714946.
† Fujian Institute of Research on the Structure of Matter, Chinese Academy of Sciences.
‡ Graduate School of the Chinese Academy of Sciences.

(1) (a) Kahn, O. *Molecular Magnetism*; VCH: Weinheim, Germany, 1993. (b) Sakamoto, M.; Manseki, K.; Ökawa, H. *Coord. Chem. Rev.* **2001**, *219*−*221*, 379. (c) Gatteschi, D.; Sessoli, R. *Angew. Chem., Int. Ed.* **2003**, *42*, 268. (d) Zheng, Y.-Z.; Tong, M.-L.; Zhang, W.-X.; Chen, X.-M. *Angew. Chem., Int. Ed.* **2006**, *45*, 6310.
(2) (a) Castillo, O.; Luque, A.; Román, P.; Lloret, F.; Julve, M. *Inorg. Chem.* **2001**, *40*, 5526. (b) Xiang, S.; Wu, X.; Zhang, J.; Fu, R.; Hu, S.; Zhang, X. *J. Am. Chem. Soc.* **2005**, *127*, 16352. (c) Wang, X.-Y.; Wang, Z.-M.; Gao, S. *Chem. Commun.* **2008**, 281.
(3) Li, J.-R.; Yu, Q.; Sañudo, E. C.; Tao, Y.; Bu, X.-H. *Chem. Commun.* **2007**, 2602.
(4) (a) Yi, L.; Ding, B.; Zhao, B.; Cheng, P.; Liao, D.-Z.; Yan, S.-P.; Jiang, Z.-H. *Inorg. Chem.* **2004**, *43*, 33. (b) Zhang, J.-P.; Zheng, S.-L.; Huang, X.-C.; Chen, X.-M. *Angew. Chem., Int. Ed.* **2004**, *43*, 206. (c) Ye, Q.; Li, Y.-H.; Huang, X.-F.; Xiong, R.-G.; Xue, Z. *Inorg. Chem.* **2005**, *45*, 3618. (d) Li, D.; Wu, T.; Zhou, X.-P.; Zhou, R.; Huang, X.-C. *Angew. Chem., Int. Ed.* **2005**, *44*, 4175. (e) Luo, T.-T.; Tsai, H.-L.; Yang, S.-L.; Liu, Y.-H.; Yadav, R. D.; Su, C.-C.; Ueng, C.-H.; Lin, L.-G.; Lu, K.-L. *Angew. Chem., Int. Ed.* **2005**, *44*, 6063. (f) Park, H.; Moureau, D. M.; Parise, J. B. *Chem. Mater.* **2006**, *18*, 5251.

10.1021/ic801026y CCC: $40.75
Published on Web 09/12/2008

ferrimagnetism, and so on.[5] With respect to tetrazolate ligands, quite a few magnetical systems including iron(II),[6] copper(II),[7] cobalt(II),[8] and iron(III) and lanthanide(III)[9] have been characterized. However, to the best of our knowledge, up to now the magnetic investigation on tetrazole-bridged manganese(II) complexes is very rare[10] because only a few polynuclear or multidimensional manganese(II) complexes of tetrazole-containing ligands have been observed, and in some cases, the magnetic studies have not been described.[11] Although numerous tetrazolate-containing complexes with spin crossover, antiferromagnetism, ferromagnetism, and ferrimagnetism have been found,[6−10] there are only two examples displaying spin-canted behavior,[12] and in particular those with spin-flop behavior have not yet been reported.

The *N*,*N*-bis[1(2)*H*-tetrazol-5-yl]amine (H_2bta) ligand as an important tetrazaolate derivative remains mostly unexplored except for the recently reported several mononuclear,[13] 1-D,[7i] and 2-D[10] coordination polymers. We choose the H_2bta ligand in the present work on the basis of the following considerations: (1) it contains nine-coordinate atoms originating from double tetrazole rings and an amine group, promising rich and versatile coordination modes to achieve diverse structures with interesting topology and unexpected magnetic behaviors; (2) it possesses three reversible diprotonated, monoprotonated, and deprotonated types of H_2bta, Hbta$^-$, and bta^{2-}, implying diverse acidity-dependent coordination modes, and (3) it is a flexible bridging ligand, favoring the formation of a helical structure. In this paper, two unprecedented manganese(II) tetrazolate complexes, $Mn_3(Hbta)_4(\mu_2\text{-}OH)_2(H_2O)\cdot 2H_2O$ (**1**) and Mn(bta)(H_2O) (**2**), were synthesized under hydrothermal conditions. Notably, the different acidity-dependent types and coordination modes of the ligand lead to distinct dimensions and architectures of the two complexes. Magnetic studies show that compound **1** exhibits an antiferromagnetical ordering with $T_N = 4.5$ K and compound **2** shows the simultaneous presence of a spin-canted antiferromagnetism and a field-induced spin-flop transition.

Experimental Section

Materials and Instruments. All chemicals were used as purchased without further purification. H_2bta was synthesized according to the literature.[7i] Powder X-ray diffraction (PXRD) patterns were obtained from a Rigaku DMAX2500 powder diffractometer at 40 kV and 100 mA using Cu Kα ($\lambda = 1.540\,56$ Å), with a scan speed of 0.375 s/step and a step size of 0.05°. The simulated PXRD patterns were calculated using single-crystal X-ray diffraction data and processed by the free *Mercury v1.4* program provided by the Cambridge Crystallographic Data Centre. Magnetic susceptibilities were acquired by using a Quantum Design PPMS model 6000 magnetometer. Elemental analyses of C, H, and N were carried out with an Elementar Vario MICRO. The Fourier transform infrared (FT-IR) spectra were measured on a Nicolet Magna 750 FT-IR spectrophotometer in the region of 4000−400 cm^{-1} using KBr pellets as bases. Thermogravimetric analyses (TGA) were investigated on a Netzsch Sta449C thermoanalyzer under a N_2 atmosphere with a ramp rate of 10 °C/min.

Preparations of 1 and 2. A mixture of $MnCl_2\cdot 4H_2O$ (85 mg, 0.8 mmol) and H_2bta (84 mg, 0.5 mmol) in 10 mL of deionized water with a starting value of pH = 3 was sealed into a 25-mL poly(tetrafluoroethylene)-lined stainless steel container under autogenous pressure, kept at 160 °C for 3 days, and then cooled to room temperature at a rate of 2.7 °C/h. Pale-red crystals of **1** were filtered off from the solution (yield 40%, based on Mn), then washed with water, and dried in air. Anal. Calcd for $C_8H_{18}Mn_3N_{36}O_6$: C, 10.93; H, 2.06; N, 57.34. Found: C, 11.08; H, 1.91; N, 56.61. IR (KBr, cm^{-1}): ν 3292 (s), 3041 (s), 2916 (s), 2789 (s), 2629 (m),

(5) (a) Fujigaya, T.; Jiang, D.-L.; Aida, T. *J. Am. Chem. Soc.* **2003**, *125*, 14690. (b) Barea, E.; Romero, M. A.; Navarro, J. A. R.; Salas, J. M.; Masciocchi, N.; Galli, S.; Sironi, A. *Inorg. Chem.* **2005**, *44*, 1472. (c) Luneau, D.; Rey, P. *Coord. Chem. Rev.* **2005**, *249*, 2591. (d) Ouellette, W.; Galán-Mascarós, J. R.; Dunbar, K. R.; Zubieta, J. *Inorg. Chem.* **2006**, *45*, 1909. (e) Zeng, M.-H.; Wang, B.; Wang, X.-Y.; Zhang, W.-X.; Chen, X.-M.; Gao, S. *Inorg. Chem.* **2006**, *45*, 7069. (f) Ouellette, W.; Prosvirin, A. V.; Chieffo, V.; Dunbar, K. R.; Hudson, B.; Zubieta, J. *Inorg. Chem.* **2006**, *45*, 9346. (g) Ouellette, W.; Prosvirin, A. V.; Valeich, J.; Dunbar, K. R.; Zubieta, J. *Inorg. Chem.* **2007**, *46*, 9067. (h) Piñero, D.; Baran, P.; Boca, R.; Herchel, R.; Klein, M.; Raptis, R. G.; Sanakis, F. R. Y. *Inorg. Chem.* **2007**, *46*, 10981.

(6) (a) Koningsbruggen, P. J.; Garcia, Y.; Kahn, O.; Fournès, L.; Kooijman, H.; Spek, A. L.; Haasnoot, J. G.; Moscovici, J.; Provost, K.; Michalowicz, A.; Renz, F.; Gu1tlich, P. *Inorg. Chem.* **2000**, *39*, 1891. (b) Stassen, A. F.; Grunert, M.; Dova, E.; Müller, M.; Weinberger, P.; Wiesinger, G.; Schenk, H.; Linert, W.; Haasnoot, J. G.; Reedijk, J. *Eur. J. Inorg. Chem.* **2003**, 2273. (c) Grunert, C. M.; Schweifer, J.; Weinberger, P.; Linert, W. *Inorg. Chem.* **2004**, *43*, 155. (d) Absmeier, A.; Bartel, M.; Carbonera, C.; Jameson, G. N. L.; Weinberger, P.; Caneschi, A.; Mereiter, K.; Létard, J.-F.; Linert, W. *Chem.—Eur. J.* **2006**, *12*, 2235. (e) Zhang, W.; Zhao, F.; Liu, T.; Yuan, M.; Wang, Z.-M.; Gao, S. *Inorg. Chem.* **2007**, *46*, 2541. (f) Bronisz, R. *Inorg. Chem.* **2007**, *46*, 6733. (g) Quesada, M.; Kooijman, H.; Gamez, P.; Costa, J. S.; Koningsbruggen, P. J.; Weinberger, P.; Reissner, M.; Spek, A. L.; Haasnoot, J. G.; Reedijk, J. *Dalton Trans.* **2007**, 5434.

(7) (a) Stassen, A. F.; Kooijman, H.; Spek, A. L.; Jongh, L. J.; Haasnoot, J. G.; Reedijk, J. *Inorg. Chem.* **2002**, *41*, 6468. (b) Stassen, A. F.; Driessen, W. L.; Haasnoot, J. G.; Reedijk, J. *Inorg. Chim. Acta* **2003**, *350*, 57. (c) Shvedenkov, Y.; Bushuev, M.; Romanenko, G.; Lavrenova, L.; Ikorskii, V.; Gaponik, P.; Larionov, S. *Eur. J. Inorg. Chem.* **2005**, 1678. (d) Gaponik, P. N.; Voitekhovich, S. V.; Lyakhov, A. S.; Matulis, V. E.; Ivashkevich, O. A.; Quesada, M.; Reedijk, J. *Inorg. Chim. Acta* **2005**, *358*, 2549. (e) Gaponik, P. N.; Degtyarik, M. M.; Lyakhov, A. S.; Matulis, V. E.; Ivashkevich, O. A.; Quesada, M.; Reedijk, J. *Inorg. Chim. Acta* **2005**, *358*, 3949. (f) Tretyakov, E. V.; Fokin, S. V.; Romanenko, G. V. *Russ. Chem. Bull.* **2006**, *55*, 66. (g) Stassen, A. F.; Grunert, M.; Mills, A. M. *Dalton Trans.* **2003**, 3628. (h) Luo, T.-T.; Tsai, H.-L.; Yang, S.-L.; Liu, Y.-H.; Yadav, R. D.; Su, C.-C.; Ueng, C.-H.; Lin, L.-G.; Lu, K.-L. *Angew. Chem., Int. Ed.* **2005**, *44*, 6063. (i) Friedrich, M.; Gálvez-Ruiz, J. C.; Klapö1tke, T. M.; Mayer, P.; Weber, B.; Weigand, J. J. *Inorg. Chem.* **2005**, *44*, 8044. (j) Zhang, X.-M.; Zhao, Y.-F.; Zhang, W.-X.; Chen, X.-M. *Adv. Mater.* **2007**, *19*, 2843. (k) Li, J.-R.; Yu, Q.; Sañudo, E. C.; Tao, Y.; Song, W.-C.; Bu, X.-H. *Chem. Mater.* **2008**, *20*, 1218. (l) Yu, Q.; Zhang, X.; Bian, H.; Liang, H.; Zhao, B.; Yan, S.; Liao, D. *Dalton Trans.* **2008**, 1140.

(8) (a) Shvedenkov, Y. G.; Virovets, A. V.; Lavrenova, L. G. *Russ. Chem. Bull.* **2003**, *52*, 1353. (b) Shvedenkov, Y. G.; Ikorskii, V. N.; Lavrenova, L. G. *J. Phys. IV* **2004**, *114*, 649.

(9) (a) Saalfrank, R. W.; Lurz, C. J.; Schobert, K. *Angew. Chem., Int. Ed.* **1991**, *30*, 1494. (b) He, F.; Tong, M.-L.; Yu, X.-L.; Chen, X.-M. *Inorg. Chem.* **200544**, 559. (c) Zhang, X.-Q.; Yu, Q.; Bian, H.-D. *Aust. J. Chem.* **2008**, *61*, 303.

(10) Gao, E.-Q.; Liu, N.; Cheng, A.-L.; Gao, S. *Chem. Commun.* **2007**, 2470.

(11) (a) Dincă, M.; Yu, A. F.; Long, J. R. *J. Am. Chem. Soc.* **2006**, *128*, 8904. (b) Dincă, M.; Dailly, A.; Liu, Y.; Brown, C. M.; Neumann, D. A.; Long, J. R. *J. Am. Chem. Soc.* **2006**, *128*, 16876. (c) Dincă, M.; Long, J. R. *J. Am. Chem. Soc.* **2007**, *129*, 11172. (d) Horike, S.; Dincă, M.; Tamaki, K.; Long, J. R. *J. Am. Chem. Soc.* **2008**, *130*, 5854.

(12) (a) Rodríguez, A.; Kivekäs, R.; Colacio, E. *Chem. Commun.* **2005**, 5228. (b) Rodríguez-Diéguez, A.; Palacios, M. A.; Sironi, A.; Colacio, E. *Dalton Trans.* **2008**, 2887.

(13) CCDC Nos. 281689, 287824, and 292437.

Table 1. Crystal Data for **1** and **2**

	1	**2**
formula	$C_8H_{18}Mn_3N_{36}O_6$	$C_6H_7MnN_9O$
fw	879.40	276.15
cryst syst	orthorhombic	monoclinic
space group	*Ibam*	$P2_1/c$
cryst size, mm^3	0.30 × 0.20 × 0.20	0.30 × 0.26 × 0.25
a, Å	9.286(6)	11.300(2)
b, Å	11.406(7)	10.077(2)
c, Å	25.70(3)	10.122(2)
β, deg		109.22(3)
V, Å^3	2723(4)	1088.4(4)
Z	4	4
D_c, g/cm^3	2.146	1.685
T, K	293(2)	293(2)
θ range, deg	3.17−25.33	3.58−27.48
total reflns	8344	4796
obsd reflns	1246	1380
params/restraints/data	134/4/1246	125/3/1380
unique reflns/R_{int}	1262/0.0138	1494/0.0282
R1[a] [$I > 2\sigma(I)$]	0.0303	0.0348
wR2[b] (all data)	0.1369	0.1269
GOF on F^2	0.981	0.998
ρ_{max}/ρ_{min}, e/Å^3	0.594/−0.640	0.812/−0.513

[a] $R1 = ||F_o| - |F_c||/|F_o|$. [b] $wR2 = [w(F_o^2 - F_c^2)^2]/[w(F_o^2)^2]^{1/2}$.

1871 (w), 1659 (vs), 1630 (vs), 1508 (vs), 1431 (m), 1319 (m), 1234 (w), 1146 (w), 1041 (m), 991 (w), 895 (w), 854 (w), 798 (m), 731 (m), 428 (w).

Colorless crystals of **2** in 20% yield (based on Mn) were obtained by a method similar to that of **1** except that 9 mL of deionized water and 1 mL of 25% $NH_3 \cdot H_2O$ were used as the solvents with a starting value of pH = 11, and then the mixture was filtered off from the solution, washed with water, and dried in air. Anal. Calcd for $C_2H_3MnN_9O$: C, 10.72; H, 1.35; N, 56.26. Found: C, 10.73; H, 1.33; N, 55.46. IR (KBr, cm^{-1}): ν 3278 (s), 3167 (m), 3089 (s), 2934 (s), 2185 (w), 1633 (s), 1551(s), 1514 (s), 1411 (m), 1336 (w), 1271 (w), 1146 (m), 1034 (w), 864 (m), 810 (s), 721 (m), 621 (m), 434 (w).

Single-Crystal Structure Determination. Single crystals were mounted on a Rigaku Mercury CCD diffractometer equipped with graphite-monochromated Mo Kα radiation (λ = 0.710 73 Å) using an ω-scan technique at 293 K. The intensity data sets were reduced by the *CrystalClear* software.[14] The structures were solved by direct methods with the Siemens *SHELXTL* version 5 package of crystallographic software[15] and refined by full-matrix least-squares techniques. Non-H atoms were located by difference Fourier maps and subjected to anisotropic refinement. H atoms were added according to theoretical models. Crystallographic data and structural refinements and selected bond distances and angles for **1** and **2** are listed in Tables 1 and 2, respectively.

TGA for 1 and 2. TGA of **1** show 21.2% weight loss in the range of 30−200 °C (Figure S1a in the Supporting Information), in agreement with the removal of solvent and coordinated water molecules per cell (12.65% calcd). Further weight losses from 200 to 500 °C correspond to decomposition of the network. The TGA curve of **2** reveals that the framework was stable between 30 and 360 °C and then weight losses occurred from 360 to 864 °C due to decomposition of the network (Figure S1b in the Supporting Information).

(14) *CrystalClear: Software User's Guide for the Rigaku R-Axis, and Mercury and Jupiter CCD Automated X-ray Imaging System*, version 1.35; Rigaku Molecular Structure Corp.: The Woodlands, TX, 2002.

(15) *SHELXTL Reference Manual*, version 5; Siemens Energy & Automation Inc.: Madison, WI, 1994.

Table 2. Selected Bond Lengths and Angles for **1** and **2**[a]

complex **1**		complex **2**	
	Bond Length		
Mn(1)−O(1W)	2.136(2)	Mn(1)−O(1W)	2.192(2)
Mn(2)−O(1)	2.359(2)	Mn(1)−N(1A)	2.276(2)
Mn(2)−N(9)	2.172(2)	Mn(1)−N(2B)	2.302(2)
Mn(1)−N(3)	2.302 (2)	Mn(1)−N(4)	2.297(2)
Mn(2)−N(1)	2.261(2)	Mn(1)−N(7C)	2.316(2)
		Mn(1)−N(9A)	2.245(2)
	Angle		
O(1W)−Mn(1)−O(1WA)	180.00(1)	O(1W)−Mn(1)−N(9A)	110.56(8)
N(9)−Mn(2)−N(1)	78.87(6)	N(9A)#1−Mn(1)−N(4)	84.04(8)
O(1W)−Mn(1)−N(3)	90.84(7)	N(6)−N(7)−Mn(1C)	116.39(16)
N(1)−Mn(2)−O(1)	97.22(8)	N(1A)−Mn(1)−N(2B)	99.73(7)
N(9)−Mn(2)−N(1D)	103.83(6)	N(2B)−Mn(1)−N(7C)	76.21(8)
N(3)−Mn(1)−N(3A)	180.00(5)	N(3)−N(4)−Mn(1)	116.56(14)
N(3B)−Mn(1)−N(3A)	94.16(9)	N(2)−N(1)−Mn(1D)	128.24(15)
N(1)−Mn(2)−O(1D)	159.04(4)	N(4)−Mn(1)−N(7C)	100.10(8)
O(1D)−Mn(2)−O(1)	73.13(10)	O(1W)−Mn(1)−N(7C)	158.06(8)
N(9)−Mn(2)−O(1)	93.63(4)	O(1W)−Mn(1)−N(1A)	85.11(8)
Mn(2E)−O(1)−Mn(2)	106.87(10)	N(9A)−Mn(1)−N(1A)	78.95(7)
C(2)−N(5)−C(1)	124.85(14)	N(9A)−Mn(1)−N(7C)	91.38(8)
		N(1)−N(2)−Mn(1E)	131.98(16)
		C(1)−N(5)−C(2)	123.5(2)

[a] Symmetry codes for **1**: (A) $-x, -y + 1, -z$; (B) $x,y, -z$; (C) $-x, -y + 1, z$; (D) $-x + 1, -y + 1, z$; (E) $-x + 1, y + 0, -z + {}^1/_2$. Symmetry codes for **2**: (A) $x - {}^1/_2, -y + {}^3/_2, z + {}^1/_2$; (B) $-x + {}^1/_2, y - {}^1/_2, -z + {}^3/_2$; (C) $-x, -y + 1, -z + 1$; (D) $x + {}^1/_2, -y + {}^3/_2, z - {}^1/_2$; (E) $-x + {}^1/_2, y + {}^1/_2, -z + {}^3/_2$.

Results and Discussion

Syntheses. As we know, in a special hydrothermal process, many factors can affect the formation and crystal growth of the product phases, such as the initial reactants, starting concentrations, solvents, pH values, reaction times, temperatures, etc. In our case, the pH value of the reaction solution is a key factor in the formation of different structural networks in **1** and **2** mainly resulting from the acidity-dependent modes of the ligand. Under acidic conditions, the ligand is monodeprotonated and adopts the $Hbta^-$ type for **1**; on the contrary, it employs the bta^{2-} dideprotonated type for **2** under the basic environment. The PXRD patterns of the bulk products are in good agreement with the calculated patterns based on the single-crystal solution, indicating the phase purity of **1** and **2** (Figure S2 in the Supporting Information).

Crystal Structures of 1 and 2. A single-crystal X-ray analysis shows that the framework of **1** features a 2-D gridlike network. In the asymmetrical unit of **1** (Figure 1), there are two crystallographically independent Mn^{II} ions, one $Hbta^-$ ligand, one hydroxyl group, one coordinated water molecule, and one solvated water molecule. The Mn1 atom is trans-coordinated by four N3 atoms from four $Hbta^-$ ligands on the equatorial plane, with Mn1−N3 = 2.302(2) Å and two terminal water molecules occupying the two axial sites with Mn1−O1W = 2.136(2) Å, yielding a compressed (4 + 2) octahedron. The Mn2 atom is cis-coordinated by two chelating $Hbta^-$ ligands with Mn2−N1 = 2.261(2) and Mn2−N9 = 2.172(3) Å and two hydroxyl groups with Mn2−O1 = 2.359(2) Å to complete a slightly distorted octahedron. In **1**, each of $Hbta^-$ ligand acts as a μ_3 linker, which coordinates to the Mn2 ion in a chelating fashion through N1 and N9 atoms from different tetrazole rings and

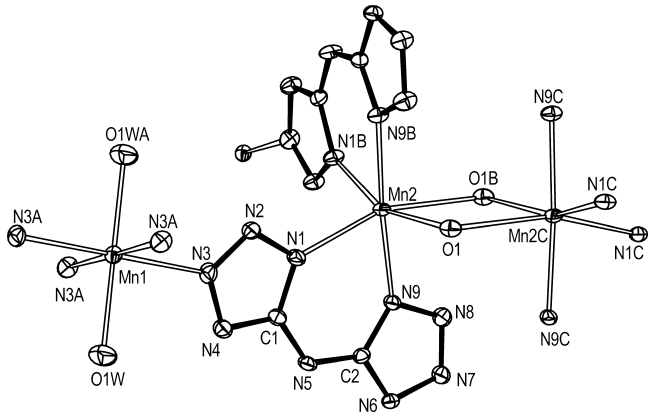

Figure 1. ORTEP drawing with 50% thermal ellipsoids of the manganese coordination environment in **1**. Symmetry codes: (A) $-x$, $1 - y$, z; (B) $1 - x$, $1 - y$, z; (C) x, $1 - y$, $^1/_2 - z$.

also bonds to a Mn1 atom via the N3 atom, presenting a similar −Mn−N1−N2−N3−Mn− end-to-end azide-bridged coordination mode to link Mn1 and Mn2 [Mn1···Mn2 = 6.487(4) Å]. The two tetrazole rings of each $Hbta^-$ ligand are almost coplanar with a small dihedral angle of 4.23(6)°; moreover, the two ligated $Hbta^-$ ligands binding to the Mn2 atom are nearly perpendicular with a dihedral angle of 86.36(3)°. Two μ_2-OH groups doubly bridge two equivalent Mn2 atoms to form a rhombus binuclear $Mn_2(\mu_2\text{-}OH)_2$ unit with a Mn2···Mn2 separation of 3.789(4) Å and a Mn2−O1−Mn2C bond angle of 106.9(1)°. Each $Mn_2(\mu_2\text{-}OH)_2(Hbta)_4$ dimer links four Mn1 centers, while each Mn1 center connects four $Mn_2(\mu_2\text{-}OH)_2(Hbta)_4$ dimers, forming a novel 2-D (4,4) topological network in the *ac* plane (Figure 2). Notably, only five complexes[16] containing $Mn_2(\mu_2\text{-}OH)_2$ units are observed in the Cambridge Structural Database, and all of them are discrete in structure. As a result, complex **1** is the first extended architecture constructed by $Mn_2(\mu_2\text{-}OH)_2$ units. Moreover, taking into account the strong hydrogen-bonding interactions [O1−H···N7, O1W−H···O2W, N5−H···N5, and N6−H···N6, with distances ranging from 2.742(4) to 2.867(6) Å and angles falling in the range of 119.2(5)−180(2)°], complex **1** can be extended to a 3-D supramolecular architecture but without open channels because the adjacent layers are arranged in an −ABAB− manner (Figure S3 in the Supporting Information).

Compound **2** crystallizes in the monoclinic space group $P2_1/c$, and its 3-D framework is constructed by binuclear $Mn_2(bta)_2$ units. There is a unique Mn atom in the asymmetric unit. Each Mn ion adopts a distorted octahedral MnN_5O geometry, with the equatorial plane consisting of four N atoms from three bta^{2-} ligands and the axial positions being occupied by one N atom from another bta^{2-} ligand and one O atom from the terminal water molecule (Figure 3). The bond lengths of Mn−N range from 2.245(2) to 2.316(2) Å and that of Mn−O is 2.192(2) Å, comparable to those in the literature.[17] Interestingly, different from that in **1**, the H_2bta ligand employs the dideprotoned bta^{2-} type under basic conditions and behaves as a pentadentate coordination mode. In the mononuclear,[13] 1-D,[7i] and 2-D[10] structures, the bta^{2-} ligand acts as a bidentate, tridentate, or tetradentate linker, respectively; however, the pentadentate coordination mode of the bta^{2-} ligand exhibited in **2** is first observed.

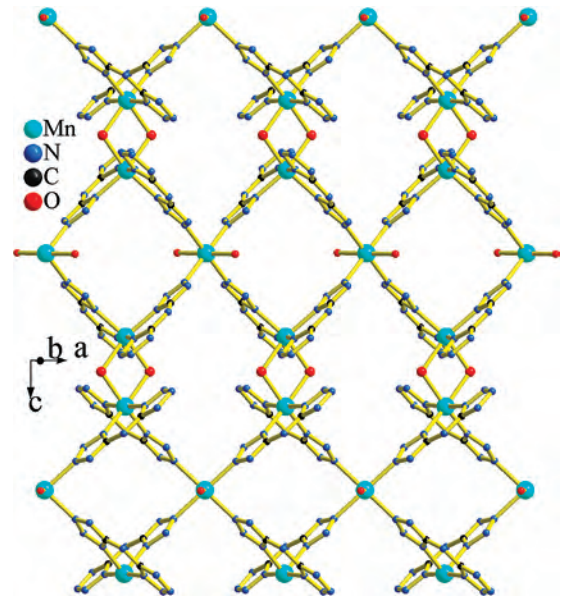

Figure 2. 2-D layer of **1** viewed along the *b* axis (H atoms are omitted for clarity).

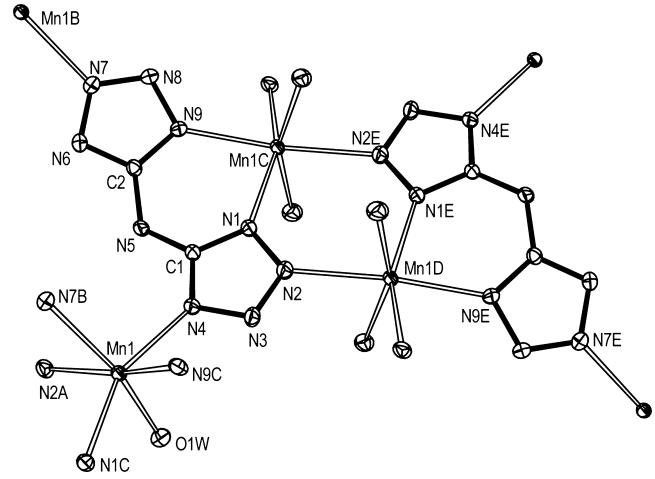

Figure 3. ORTEP view with 50% thermal ellipsoids of the $Mn_2(bta)_2$ core in **2**. Symmetry codes: (A) $^1/_2 - x$, $-^1/_2 - y$, $^3/_2 - z$; (B) $-x$, $1 - y$, $1 - z$; (C) $-^1/_2 - x$, $^3/_2 + y$, $^1/_2 + z$; (D) $^1/_2 - x$, $^1/_2 + y$, $^3/_2 - z$; (E) $1 - x$, $2 - y$, $1 - z$.

In **2**, each bta^{2-} ligand is bonded to four Mn atoms, with N1 and N9 atoms chelating the Mn1C center, the N2 atom binding the neighboring Mn1D atom, and N4 and N7 atoms connecting the other two Mn (Mn1 and Mn1B) centers, thus setting up two end-to-end azide-like linkages (−Mn−N2−N3−N4−Mn− and −Mn−N7−N8−N9−Mn−) in each

(16) (a) Maslen, H. S.; Waters, T. N. *Chem. Commun.* **1973**, 760. (b) Kitajima, N.; Singh, U. P.; Amagai, H.; Osawa, M.; Moro-oka, Y. *J. Am. Chem. Soc.* **1991**, *113*, 7757. (c) Zhang, X.-Y.; O'Connor, C. J.; Jameson, G. B.; Pope, M. T. *Inorg. Chem.* **1996**, *35*, 30. (d) Si, S.-F.; Tang, J.-K.; Liao, D.-Z.; Jiang, Z.-H.; Yan, S.-P. *J. Mol. Struct.* **2002**, *606*, 87. (e) Mialane, P.; Duboc, C.; Marrot, J.; Riviere, E.; Dolbecq, A.; Secheresse, F. *Chem.—Eur. J.* **2006**, *12*, 1950.

(17) (a) Mautner, F. A.; Gspan, C.; Gatterer, K.; Goher, M. A. S.; Abu-Youssef, M. A. M.; Bucher, E.; Sitte, W. *Polyhedron* **2004**, *23*, 1217. (b) Lin, P.; Clegg, W.; Harrington, R. W.; Henderson, R. A. *Dalton Trans.* **2005**, 2388.

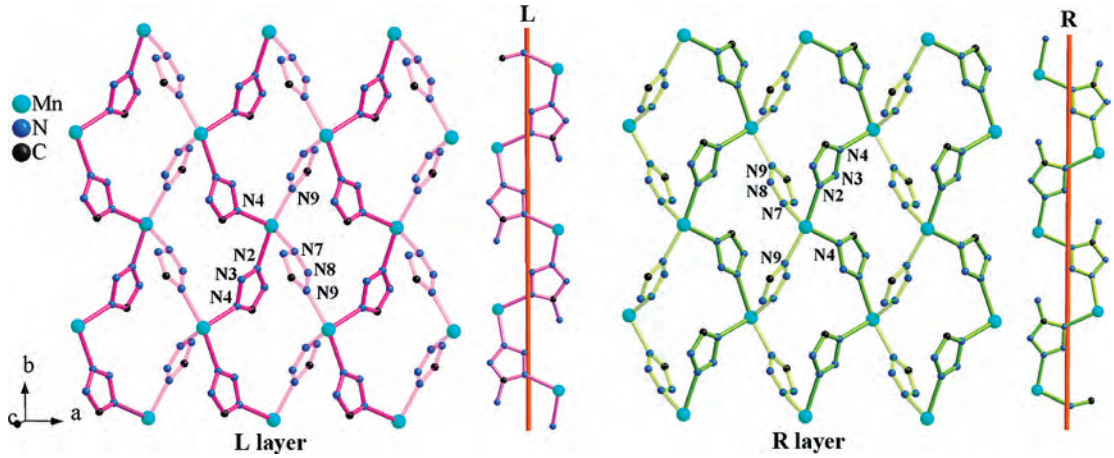

Figure 4. Plots of the (a) left-handed and (b) right-handed chiral layers constructed by the two types of helical chains in **2**.

tetrazole ring. The dihedral angle between the two tetrazole rings is 19.64(6)°, which is larger than that in **1**. As shown in Figure 3, two Mn1 atoms are connected by two bta^{2-} ligands to construct a dimeric $Mn_2(bta)_2$ unit, in which two MnC_2N_3 six-membered rings are built through each bta^{2-} ligand chelating one Mn1 atom and one Mn_2N_4 six-membered ring is constructed through two N1-containing tetrazole rings doubly bridging two Mn1 atoms. The similar M_2N_4 six-membered rings were previously found in two tetrazolate-bridged zinc(II) complexes.[18] The Mn···Mn separations connected by double-bridging N1-containing tetrazole rings and by the above-mentioned end-to-end azide-like bridging mode are 4.295(3) and 6.243(1) Å, respectively.

Notably, the adjacent $Mn_2(bta)_2$ units are interrelated by a 2_1-screw operation. To shed light on the helix and the structure of **2**, we first omit the N5−C1/C2 bonds in the bta^{2-} ligands and the Mn1−N1 bonds. As shown in Figure 4, each helical chain can be described as $(-Mn-N-N-N-)_n$, and there are two types of helices (−Mn−N2−N3−N4−Mn− and −Mn−N7−N8−N9−Mn−) from the two tetrazole rings in each bta^{2-} ligand. The pitch of the 2_1 helix is about 9.711 Å along the *b* axis. The two types of helical chains with the same handness are interwoven via Mn atoms as hinges to extend into a 2-D chiral layer with left- or right-handness (parts a and b of Figure 4, respectively). As shown in Figure 5, these chiral layers are stacked alternately through Mn1−N1, N5−C1, and N5−C2 bonds to form a 3-D network of **2** with nonchirality. It is noteworthy that compound **2** represents the first bta-bridged complex featuring a 3-D structure. Taking into account each bta^{2-} ligand and the Mn center as four nodes, the framework of **2** exhibits a distorted 3-D PtS net with the Schläfli topological notation for 4^28^4, in which the long vertex symbols for the four-connecting-node bta^{2-} ligands and Mn centers are $4.4.8_2.8_2.8_8.8_8$ and $4.4.8_7.8_7.8_7.8_7$, respectively.[19]

Magnetic Properties. The plots of the χ_M and $\chi_M T$ vs T and the fitting line under a 5 kOe external field for **1** are shown in Figure 6. The $\chi_M T$ value at 300 K is 12.76 emu·K/mol, being close to the spin-only value of 13.12 emu·K/mol expected for three magnetically isolated high-spin Mn^{II} ions considering $g = 2.00$. During cooling, the value of $\chi_M T$ continues to slowly decrease until near 100 K; below this temperature, the $\chi_M T$ value decreases sharply to 1.04 emu·K/mol at 2 K, suggesting antiferromagnetic behavior. The appearance of a round peak in the χ_M vs T curve indicates

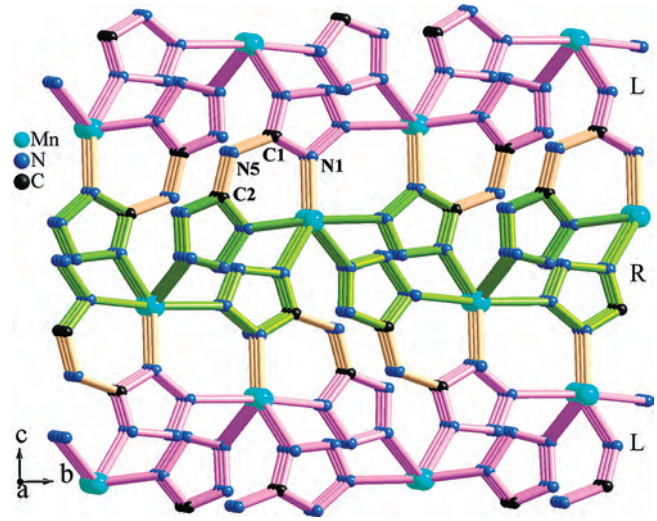

Figure 5. View the 3-D network of **2** along the *a* axis (pale red for right-handed layers and green for left-handed layers, and O atoms are omitted for clarity).

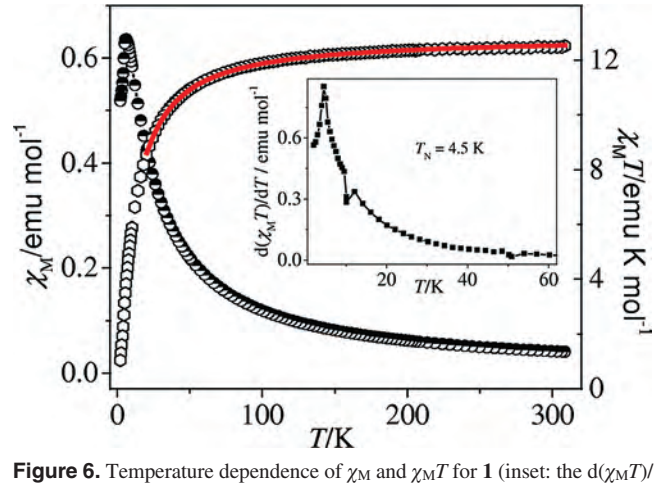

Figure 6. Temperature dependence of χ_M and $\chi_M T$ for **1** (inset: the $d(\chi_M T)/dT$ vs T derivative curve).

(18) Rodríguez-Diéguez, A.; Colacio, E. *Chem. Commun.* **2006**, 4140.
(19) Montney, M. R.; Krishnan, S. M.; Supkowski, R. M.; LaDuca, R. L. *Inorg. Chem.* **2007**, *46*, 7362.

antiferromagnetic ordering. The magnetic susceptibility data in the temperature range of 20−300 K can be well fitted to the Curie−Weiss law expression with $C = 13.15$ emu·K/mol and $\theta = -10$ K, which further confirms an overall antiferromagnetic interaction between the Mn^{II} ions. The Neel temperature, $T_N = 4.5$ K, was determined from the sharp peak in $d(\chi_M T)/dT$ (Figure 6, inset).

To quantitatively analyze the magnetic behavior of **1**, we assume that the magnetic coupling of **1** is dominated by the $Mn_2(\mu_2\text{-}OH)_2$ core constituted by two Mn2 ions and the Mn1 ion is treated as a paramagnetic ion on the basis of the structure analysis, in which the separation of Mn2···Mn2 [3.789(4) Å] connected by double OH^- bridges is much shorter than that of Mn1···Mn2 [6.487(4) Å] by three N atoms of the tetrazole ring. Accordingly, the molar magnetic susceptibility (χ) of **1** can be described as $\chi = \chi_C + (5/2)(7/2)(Ng^2\beta/3KT)$, in which $\chi_C = (2Ng^2\beta^2/KT)(A/B)$ is for the Mn_2 dimer[20] based on the isotropic spin Hamiltonian with $H = -2JS_1S_2$ and the latter is the contribution of a paramagnetic Mn1 ion. Moreover, considering the intermolecular interactions (zJ'), the magnetic data between 20 and 300 K can be well fitted using the following expression:

$$\chi_M = \chi/(1 - zJ'\chi/Ng^2\beta^2) \quad (1)$$

$$A = e^{2y} + 5e^{6y} + 14e^{12y} + 30e^{20y} + 55e^{30y} \quad (2)$$

$$B = 1 + 3e^{2y} + 5e^{6y} + 7e^{12y} + 9e^{20y} + 11e^{30y} \quad (3)$$

where $y = J/KT$. The best-fitting parameters obtained are $g = 1.98$, $J = -1.36$ cm^{-1}, and $zJ' = -0.004$ cm^{-1}. The agreement factor R, defined as $\sum[(\chi_M T)_{obsd} - (\chi_M T)_{calcd}]^2/\sum(\chi_M T)_{obsd}^2$, is equal to 6.0×10^{-4}. The negative J value reveals that dimeric Mn^{II} spins connected by double μ_2-hydroxo bridging are antiferromagnetic coupling in **1**, which is consistent with most of doubly oxygen-bridged dimanganese(II) complexes.[21,16b]

At low-temperature region of 2−20 K in the low external field of 100 Oe, the curves of field-cooled (FC) and zero-field-cooled (ZFC) magnetizations (Figure 7) are identical, confirming an antiferromagnetic ordering. Furthermore, the real part (χ') of the alternating current (ac) magnetic susceptibility in **1** has a maximum, and the imaginary part (χ'') of the ac magnetic susceptibility is negligibly small (Figure S4a in the Supporting Information). No frequency dependence was observed in the ac measurements. This also supports the conclusion that compound **1** possesses a magnetic transition phase. At 2 K in the applied field of up to 70 kOe, the field dependence of magnetization increases almost linearly, reaching 8.48 $N\beta$ at 70 kOe (Figure S5a in the Supporting Information), which is far from the saturation value of 15 $N\beta$ for three Mn^{II} ions ($S = 5/2$). This behavior is characteristic of antiferromagnetic exchange coupling.

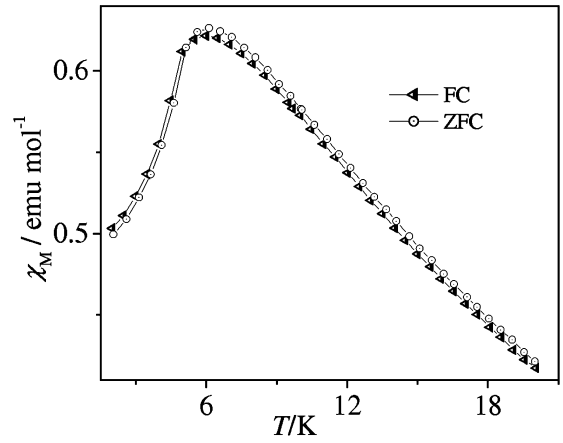

Figure 7. FC and ZFC ($H = 100$ Oe) magnetization for **1**.

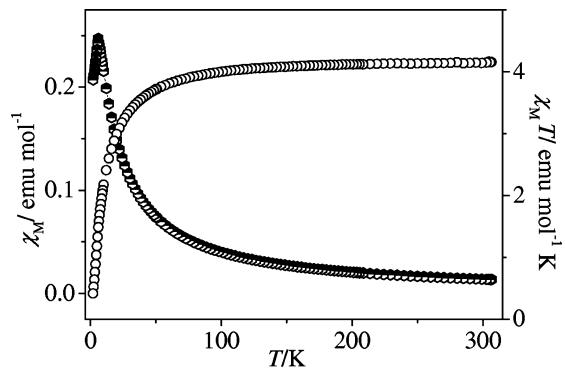

Figure 8. Temperature dependence of χ_M and $\chi_M T$ for **2**.

The magnetic susceptibility of **2** is presented in Figure 8. The temperature dependence of the reciprocal susceptibility (χ_M^{-1}) above 20 K obeys the Curie−Weiss law, with a Curie constant of $C = 4.47$ emu·K/mol and a Weiss constant of $\theta = -9.7$ K. The C value is consistent with the value of 4.37 emu·K/mol expected for a magnetically isolated high-spin Mn^{II} ion considering $g = 2.00$, while the negative θ value suggests a dominant antiferromagnetic coupling among the Mn^{II} ions. At an applied field of 5000 Oe, $\chi_M T$ decreases slowly as the temperature is decreased to 60 K and then starts to decrease sharply to 2 K. A peak at ca. 6.0 K in the $\chi_M - T$ plot is characteristic for phase transition to an antiferromagnetically ordered structure. However, the magnetic behavior of **2** is more complex in low fields. As shown in Figure 9, upon exposure to a magnetic field of 50 Oe, the value of $\chi_M T$ first decreases to a minimum at ca. 6 K as the T decreases and then increases to reach a maximum at 4.3 K and finally decreases upon further cooling. Interestingly, the magnetic behavior of **2** is highly dependent on the applied field, and the maximum around 4.3 K in the $\chi_M T - T$ curve goes down as the field increases. These features are typical for spin-canted antiferromagnetism,[22] in which a predominantly antiferromagnetic phase possesses a spontaneous

(20) Cheng, L.; Zhang, W.-X.; Ye, B.-H.; Lin, J.-B.; Chen, X.-M. *Eur. J. Inorg. Chem.* **2007**, 2668, and references cited therein.
(21) (a) Kennedy, B. J.; Murray, K. S. *Inorg. Chem.* **1985**, *24*, 1552. (b) Yu, S.-B.; Wang, C.-P.; Day, E. P.; Holm, R. H. *Inorg. Chem.* **1991**, *30*, 4067–4074. (c) Higuchi, C.; Sakiyama, H.; Okawa, H.; Isobe, R.; Fenton, D. E. *J. Chem. Soc., Dalton Trans.* **1994**, 1097. (d) Aono, T.; Wada, H.; Yonemura, M.; Ohba, M.; Okawa, H.; Fenton, D. E. *J. Chem. Soc., Dalton Trans.* **1997**, 1527. (e) Sakiyama, H.; Sugawara, A.; Sakamoto, M.; Unoura, K.; Inoue, K.; Yamasaki, M. *Inorg. Chim. Acta* **2000**, *310*, 163. (f) Sanders, C. J.; O'Shaughnessy, P. N.; Scott, P. *Polyhedron* **2003**, *22*, 1617. (g) Dubois, L.; Xiang, D.-F.; Tan, X.-S.; Pecaut, J.; Jones, P.; Baudron, S.; Pape, L. L.; Latour, J.-M.; Baffert, C.; Chardon-Noblat, S.; Collomb, M.-N.; Deronzier, A. *Inorg. Chem.* **2003**, *42*, 750.

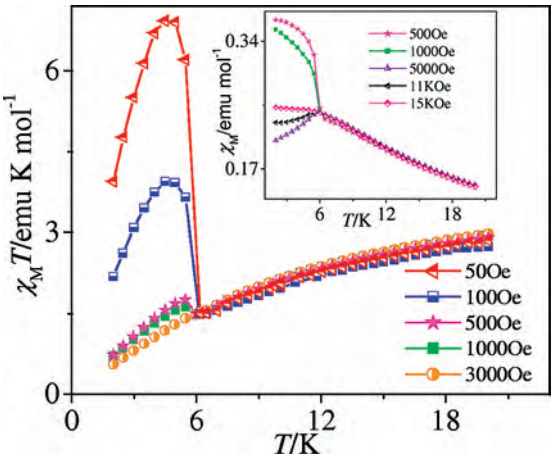

Figure 9. Plots of $\chi_M T$ vs T at different fields for **2**. Inset: plots of χ_M vs T under various fields.

magnetization originating from a small deviation between the antiparallel alignment of the spins. The disappearance of the peak at ca. 6 K in the $\chi_M - T$ plot at a higher applied field (Figure 9, inset) suggests the occurrence of a field-induced spin-flop transition.[23] The ac susceptibility (Figure S4b in the Supporting Information) shows a maximum at 6 K in the in-phase (χ') region, and a peak is also detectable in the out-of-phase (χ'') region at the same temperature. The nonzero signal in the imaginary component indicates the presence of a weak ferromagnetism as a result of the spin canting in this magnetic system. Furthermore, the absence of a frequency dependence of ac susceptibility precludes the possibility of the spin glass in **2**.

At 2 K, the field dependence of the magnetization increases almost linearly to the highest field measured of 50 kOe (Figure S5b in the Supporting Information), and no obvious sigmoid-shaped curve is observed. The magnetization value is 2.25 $N\beta$ at 50 kOe, far from the saturation value of 5 $N\beta$ for a Mn^{II} ion ($S = {}^5/_2$), which is in agreement with an antiferromagnet. In addition, a hysteresis loop is observed at 2 K with a coercive field (H_c) of 244 Oe and a remnant magnetization (M_r) of 0.014 $N\beta$ (Figure 10). This result further suggests the existence of spontaneous magnetization in **2**, being consistent with the spin-canted antiferromagnetic behavior. The canting angle is calculated to be ca. 2.72(3)°, based on the equation $\theta = \tan^{-1}(M_r/M_s)$.[3,24] The critical field of the spin-flop transition is determined by a clear discontinuity in the dM/dH curve (Figure S5b, inset, in the Supporting Information). The appearance of a maximum around 12.3 kOe in the χ' vs H curve measured at 2 K further confirms the presence of the magnetic phase transition for **2** (Figure 11).

Generally, spin canting can arise from two contributions: (1) the presence of an antisymmetric exchange and (2) the

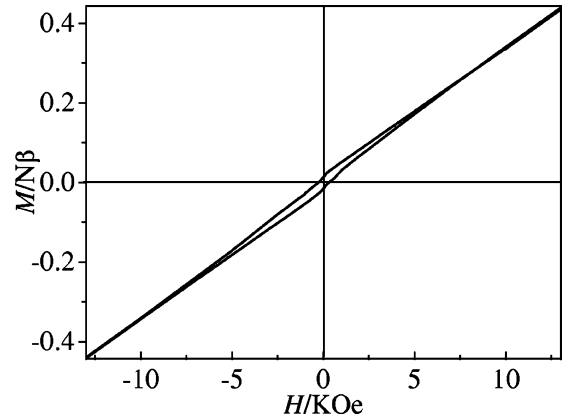

Figure 10. Hysteresis loop for **2** at 2.0 K.

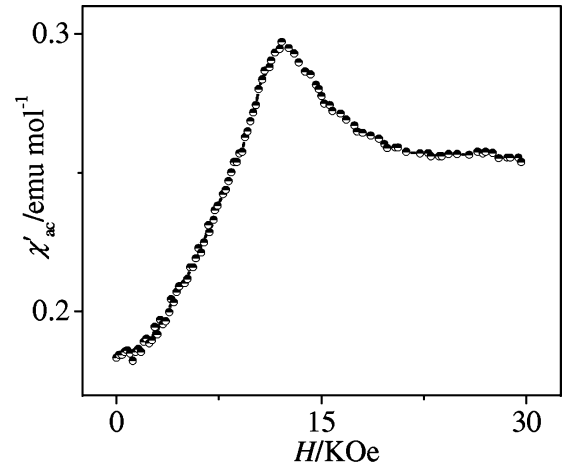

Figure 11. Field-dependent ac magnetic susceptibilities of **2** measured at 2 K.

existence of single-ion magnetic anisotropy.[25] It is well-known that the presence of an inversion center between adjacent spin centers can result in the disappearance of the antisymmetric exchange.[26] However, several high-spin manganese(II) complexes with inversion centers exhibiting spin-canted behavior have been reported in spite of the lack of antisymmetric exchange and the isotropic Mn^{II} ion, which was regarded as likely arising from weak single-ion anisotropy of the Mn^{II} site or anisotropy of the whole crystal to be considered.[27] In **1**, spin canting is not observed because of the existence of an inversion center in the $Mn_2(\mu_2\text{-}OH)_2$ core, while in **2**, although the adjacent spin Mn^{II} ions are related to a crystallographic inversion center, all of the $Mn_2(bta)_2$ dimers are connected by 2_1 helices with opposite chirality. The different orientations of opposite chirality may induce the occurrence of antisymmetric exchange, thus resulting in spin canting. Similar phenomena have been observed in several manganese azide complexes with the

(22) (a) Gutschke, S. O. H.; Price, D. J.; Powell, A. K.; Wood, P. T. *Angew. Chem., Int. Ed.* **1999**, *38*, 1088. (b) Humphrey, S. M.; Wood, P. T. *J. Am. Chem. Soc.* **2004**, *126*, 13236. (c) Huang, Y.-G.; Yuan, D.-Q.; Pan, L.; Jiang, F.-L.; Wu, M.-Y.; Zhang, X.-D.; Wei, W.; Gao, Q.; Lee, J. Y.; Li, J.; Hong, M.-C. *Inorg. Chem.* **2007**, *46*, 9609.
(23) Feng, M. L.; Prosvirin, A. V.; Mao, J. G.; Dunbar, K. R. *Chem.—Eur. J.* **2006**, *12*, 8312.
(24) Palacio, F.; Andres, M.; Horne, R.; Duyneveldt, A. J. *J. Magn. Magn. Mater.* **1986**, *54*, 1487.
(25) (a) Manson, J. L.; Kmety, C. R.; Palacio, F.; Epstein, A. J.; Miller, J. S. *Chem. Mater.* **2001**, *13*, 1068. (b) Jia, H.-P.; Li, W.; Ju, Z.-F.; Zhang, J. *Chem. Commun.* **2008**, 371.
(26) (a) Moriya, T. *Phys. Rev.* **1960**, *120*, 91. (b) Armentano, D.; Munno, G. D.; Lloret, F.; Palli, A. V.; Julve, M. *Inorg. Chem.* **2002**, *41*, 2007.
(27) (a) Schlueter, J. A.; Manson, J. L.; Hyzer, K. A.; Geiser, U. *Inorg. Chem.* **2004**, *43*, 4100. (b) Wang, X.-Y.; Wang, L.; Wang, Z.-M.; Su, G.; Gao, S. *Chem. Mater.* **2005**, *17*, 6369.

same space group,[28] in which a screw chain with opposite chirality between neighboring Mn_2 subunits also leads to spin canting. In light of Robison's expression $\sigma^2 = \sum_{i=1}^{12}(\theta_i - 90)^2/11$, where θ_i are the bond angles of the octahedron,[29] the square difference of the bond angles (σ^2) of the $Mn1^{II}$ coordination octahedron in **2** is 119.3, which shows a clear and great distortion of the $Mn1^{II}$ octahedron. Therefore, local single-ion anisotropy of $Mn1^{II}$ originating from the distorted octahedron enhances the antisymmetric interaction,[30] which might also contribute to spin canting.

In summary, the diversities of deprotonated types and coordination modes of the H_2bta ligand generate different structural networks and further lead to distinct magnetic properties. The 2-D gridlike layer of **1** behaves as antiferromagnetic ordering with $T_N = 4.5$ K, while the 3-D PtS-like framework of **2** displays the coexistence of spin canting and spin-flop transition. These studies show that tetrazolate bridging ligands are particularly promising for the design of extended networks exhibiting different and interesting bulk magnetic behaviors. The research on other metal complexes of the H_2bta ligand and their magnetic studies are in process.

Acknowledgment. We gratefully acknowledge financial support by the NSF of China (Grants 20521101 and 20701037), the NSF for Distinguished Young Scientist of China (Grant 20425104), and the NSF of Fujian Province (Grant 2006L2005).

Supporting Information Available: TGA plots, PXRD patterns, ac susceptibility measurements, field dependence of magnetization, and IR spectra for **1** and **2**, view of the −ABAB− arrangement for **1**, and X-ray crystallographic data in CIF format. This material is available free of charge via the Internet at http://pubs.acs.org.

IC801026Y

(28) Gao, E.-Q.; Yue, Y.-F.; Bai, S.-Q.; He, Z.; Zhang, S.-W.; Yan, C.-H. *Chem. Mater.* **2004**, *16*, 1590.
(29) Robison, K.; Gibbs, G. V.; Ribbe, P. H. *Science* **1971**, *172*, 567.
(30) Wang, X.-T.; Wang, Z.-M.; Gao, S. *Inorg. Chem.* **2007**, *43*, 10452.